Strong seismic heterogeneity in layer 2A near hydrothermal vents at the Mid-Atlantic Ridge

A. F. Arnulf, S. C. Singh, A. J. Harding, G. M. Kent, W. Crawford

Strong seismic heterogeneity in layer 2A near hydrothermal vents at the Mid-Atlantic Ridge

A. F. Arnulf,[1] S. C. Singh,[1] A. J. Harding,[2] G. M. Kent,[3] and W. Crawford[1]

Received 12 April 2011; revised 26 May 2011; accepted 31 May 2011; published 15 July 2011.

[1] We present a high-resolution 3D seismic image beneath the Lucky Strike volcano on the Mid-Atlantic Ridge using streamer tomography. To obtain a high-resolution ray coverage in layer 2A, we first downward continue the multichannel seismic (MCS) data close to the seafloor generating a synthetic ocean bottom experiment (SOBE) and then apply 3D travel-time tomography. We find that the upper crust is laterally heterogeneous on 2–3 km scale, with unusually low velocities (1.8–2.2 km.s^{-1}) in the upper few hundred meters beneath the Lucky Strike volcanic edifices, but normal layer 2A velocities (2.2–3.0 km.s^{-1}) beneath the lava lake. The low velocities could be due to extremely high porosity (25–50%) in recently erupted, highly fractured pillow lavas. The hydrothermal vent fields seem to lie at the boundary between the high-porosity edifices and the lower porosity lava lake. We have also imaged a reflector at the base of the volcanic edifices that is distinct from the deeper high-velocity gradient transition zone from layer 2A to 2B imaged so far. The new technique provides an image of the oceanic crust with resolutions comparable to that of seafloor geology, leading to new insight about volcanic and hydrothermal processes. **Citation:** Arnulf, A. F., S. C. Singh, A. J. Harding, G. M. Kent, and W. Crawford (2011), Strong seismic heterogeneity in layer 2A near hydrothermal vents at the Mid-Atlantic Ridge, *Geophys. Res. Lett.*, *38*, L13320, doi:10.1029/2011GL047753.

1. Introduction

[2] The surficial layer of the oceanic crust is formed by a heterogeneous process of magmatic eruptions and tectonic deformation. Historically, it has been difficult to obtain seismic images of this region with resolutions comparable to the length scales of geologic processes. As a consequence, questions remain about the relationship between seismic and geologic descriptions of the upper crust, notably the geological significance of seismic layers 2A [*Christeson et al.*, 2007]. Drilling could be used to bridge the resolution gap but on its own would be prohibitively expensive. We combine a synthetic ocean bottom experiment (SOBE) [*Harding et al.*, 2007] with three-dimensional seismic tomography to image the uppermost crust of the Lucky Strike volcano, on the Mid-Atlantic Ridge (MAR). The data are from the 2005 SISMOMAR experiment, where both seismic reflection and ocean bottom seismometer data were acquired onboard the French R/V L'Atalante to study the Lucky Strike segment. Here we present high-resolution 3D velocity structure from seafloor down to 1 km depth using the first arrival tomography of SOBE data.

[3] The Lucky Strike segment is located at 37°N on the Mid-Atlantic Ridge (MAR) south of the Azores triple junction between the Menez Gwen and North Famous segments. It is a 70 km long segment bounded to the north and south by non-transform offsets, and is spreading at a rate of 2.1 cm/y [*DeMets et al.*, 1994]. The 15–20 km wide axial valley is typical of a slow spreading ridge [*Detrick et al.*, 1995] with rough seafloor relief along axis; the bathymetry increases from 1550 m at the center of the segment to >4000 m at the nodal basins near the segment ends. Two major normal faults bound the rift valley, with vertical throws of >500–900 m [*Detrick et al.*, 1995] and there is a bulge >6 km in diameter at segment center containing three summit volcanic cones and a lava lake at its center (Figure 1a). The volcanoes show evidence of recent eruptions and faulting whereas the lava lake remains unfaulted [*Ondréas et al.*, 1997, 2009; *Humphris et al.*, 2002] and surrounded by active hydrothermal vent fields [*Langmuir et al.*, 1997].

2. Downward Extrapolation and 3-D Tomographic Inversion

[4] The 3D multichannel reflection survey contains 39 seismic lines with a shot spacing of 37.5 m and a line spacing of 100 m [*Singh et al.*, 2006a]. The shots were recorded on a ~4.5-km-long, 360-channel digital streamer and 25 ocean bottom seismometers (OBSs). The seismic reflection data imaged a 7 km long and 3–4 km wide axial magma chamber (AMC) [*Singh et al.*, 2006a], ~3.2 km below the seafloor. Moreover, OBS-based tomographic studies [*Seher et al.*, 2010a, 2010b] have revealed two low-velocity regions within the median valley: a zone above the AMC that may correspond to high-porosity volcanic formations [*Seher et al.*, 2010b], and a lower crustal zone below the axial melt lens that may reveal a region of partial melt [*Seher et al.*, 2010a]. However, the sparse OBS spacing does not allow imaging of detailed velocity structure of the shallow crust (<500 m) [*Seher et al.*, 2010b].

[5] Multichannel seismic (MCS) profiling is one of the most efficient methods for imaging the 3D structure of oceanic crust [*Kent et al.*, 2000; *Singh et al.*, 2006a, 2006b]. However, the only reflection usually imaged in the oceanic upper crust is from the base of layer 2A and this event comes from stacking, at longer offset, the wide-angle reflections/refractions from a vertical velocity gradient. The unusual wide-angle nature of the event means that depth and velocity are more poorly constrained than is the norm for pre-critical

[1] Laboratoire de Géosciences Marines, Institut de Physique du Globe de Paris, Paris, France.
[2] Cecil H. and Ida M. Green Institute of Geophysics and Planetary Physics, University of California, San Diego, La Jolla, California, USA.
[3] Nevada Seismological Laboratory, University of Nevada, Reno, Nevada, USA.

0094-8276/11/2011GL047753

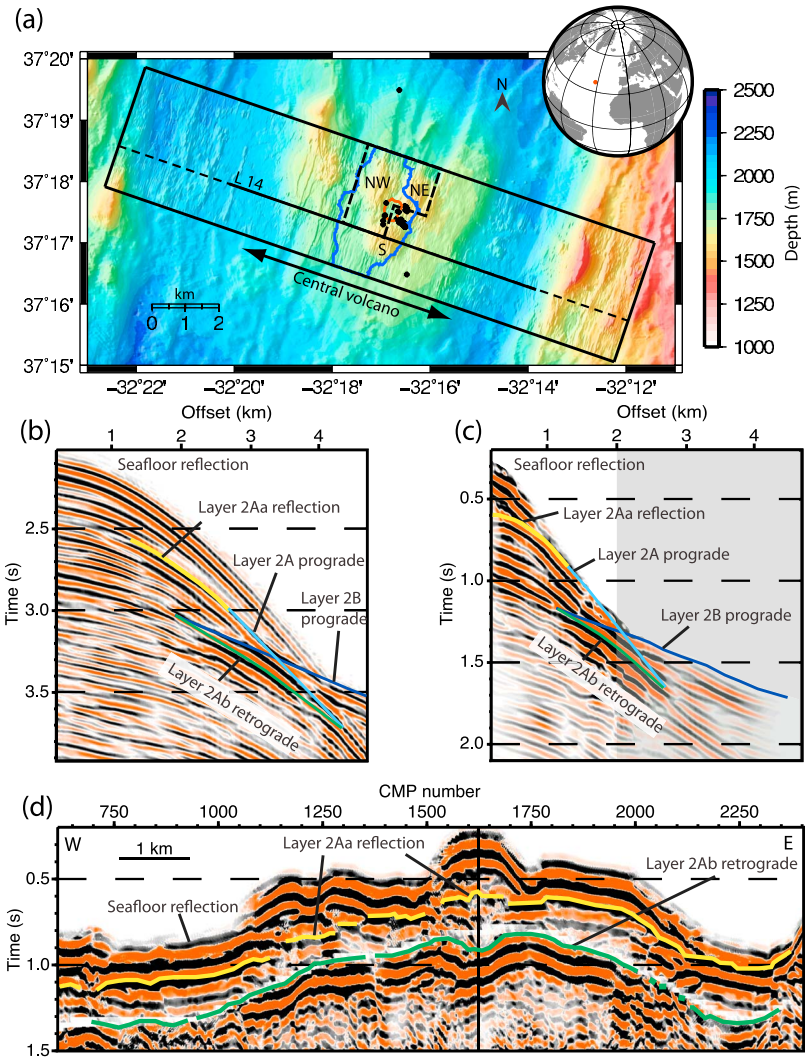

Figure 1. Study area and detailed seismic sections from line 14. (a) Bathymetric map of the central part of the Lucky Strike Segment. Southern (S), North Western (NW) and North Eastern (NE) volcanic cones. The red and blue lines show the extent of lava lake and the Axial Magma Chamber, respectively [*Combier*, 2007]. The black rectangle marks the extent of the SISMOMAR 3D survey. The extent of the sections from line 14 in Figure 2 is shown by the solid black line. The dashed black box marks the extent of Figure 4. Black circles over the volcano mark the hydrothermal vents. The inset globe shows the Lucky Strike Segment in the Atlantic Ocean. (b) Common-midpoint (CMP) gather recorded on the surface with the corresponding arrivals. (c) Same CMP gather downward continued to 1365 m below the surface. The gray zone corresponds to the unstacked part of the data. (d) Stacked seismic section of the shallow crust for line 14 produced using data downward continued 1365 m below the surface. Vertical thin black line marks the location of the CMP presented in Figures 1b and 1c.

reflections. Furthermore, the gradational transition means there is no interface to unambiguously define the layer thickness [*Harding et al.*, 1993]. These uncertainties in thickness make it harder to judge whether the base of layer 2A is an alteration front, the lava-dike transition or a combination thereof [*Christeson et al.*, 2007]. In order to resolve these ambiguities, one requires high-resolution velocity information in the first 500 m below the seafloor. Traditionally this could only be achieved by deploying both sources and receivers on the seafloor, for example in a NOBEL experiment [*Christeson et al.*, 1994]. Even then, there is still the problem achieving adequate horizontal resolution as seafloor receiver spacing is on the order of ~1 km [*Collins et al.* 2009]. Since the seismic wavefield recorded in modern MCS experiments is finely sampled, and the water velocity is very accurately known, one can downward continue [*Berryhill*, 1984] these wavefields (both source and receivers) to the seafloor, creating a Synthetic On Bottom Experiment (SOBE) whose geometry mimics a purely on-bottom experiment such as NOBEL [*Christeson et al.*, 1994], but with orders of magnitude greater sampling - a reversed 2-km-long NOBEL experiment may generate around 100 travel times [*Collins et al.*, 2009] while a similar length of MCS profiling can yield 10,000 picks. The downward extrapolation has a several advantages. First, it collapses the seafloor diffractions improving the imaging condition. Second, it causes turning ray arrivals from the upper crust to become first arrivals that can be followed from nearly zero source-receiver offset out to far ranges (Figures 1b and 1c

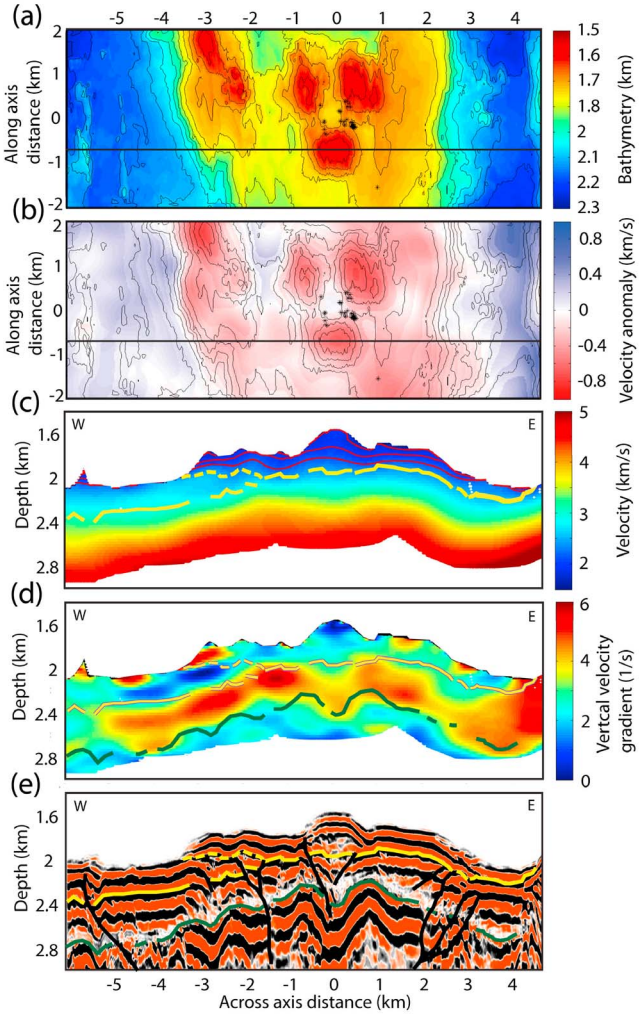

Figure 2. Upper crustal velocity structure of the Lucky Strike volcano. (a) Bathymetric map of the Lucky Strike volcano. Thin black line marks the location of line 14 shown in Figures 2c–2e. Black stars mark the hydrothermal vents. (b) Velocity anomaly map at 0.3 km bsf. (c) Velocity section. The thin red lines correspond to the velocity horizons 1.8, 2.0, 2.2 km.s^{-1}. (d) Vertical velocity gradient. (e) Depth converted stack section. Yellow lines mark the layer 2Aa boundary, dashed yellow lines correspond to shallow lava flows, green lines correspond to layer 2Ab boundary and black lines show inferred faults.

and Figure S1 of the auxiliary material), providing information about velocities from close to the seafloor down to 1 km, near the top of layer 2B (Figure 1c).[1] Furthermore, the differential moveout of reflection arrivals is enhanced near to the seafloor, leading to improved velocity analysis and imaging. Figures 1d and S2 present different reflection images of the central volcano produced by stacking the first 25 traces from the downward propagated data. In addition to the usual strong layer 2A reflector at depth (marking the transition between layer 2A and B), there is a new shallower reflector imaged at 100–250 m below the seafloor, which we will call layer 2Aa. This reflector is most clearly seen beneath the volcano edifices, and may correspond to the boundary between lava sequences of different ages. We call the second deeper reflector 2Ab, which corresponds to conventional layer 2A. It should be noted that the layer 2A 'reflection' is typically the result of stacking the caustic energy from a high gradient transition rather than being a true reflection from an interface [*Harding et al.*, 1993]. Similarly here the extra 2Aa reflection will, in general, correspond to the base of a secondary high gradient region within layer 2A (Figure S3). In some places, though, the gradient zones may be close to being true interfaces. For example, in the gather present in Figure 1, energy from the 2Aa and b events can be traced to zero offset.

[6] In order to carry out the first arrival, travel-time tomography and imaging, the 3D MCS data were downward continued to 1.3–1.7 km below the sea surface. Times of first arrivals were picked for every 5th shot (150 m) and all receivers (12.5 m) with offsets between 500 and 4000 m. Starting from a 1D velocity model, 2D models were obtained along each profile, and then combined into a starting model for 3D tomography. The data were fit to a root mean square value of ~12 ms (Figure S4), which represented the accuracy of travel-time picking. Finally, we performed several checkerboard tests with features of different sizes to assess the resolution of the velocity model in the depth range between 100 and 900 m below the seafloor. An example of these tests is shown in Figure S5.

3. Interpretation and Discussion

[7] Slices from the resulting 3D velocity model are shown in Figures 2, S6, and S7. Map sections through the velocity cube show a low velocity zone below the main central volcano (Figures 2a and 2b). Extremely low velocities (1.8 to 2.2 km.s^{-1}) are observed within the three summit cones of the Lucky Strike volcanic edifice and down to 300 m below the seafloor (Figures 2c). Velocity anomaly maps and slices show a narrow vertical zone of slightly higher velocities and probably lower porosities below the lava lake at the core of the hydrothermal vent field (Figures 2b and S6). This sharp contrast in velocity and porosity can be explained by variations of the fracture density or differences in the nature of lavas (dike, massive flows, pillow lavas), or even a combination of these two factors. Slice sections through the model also reveal a high velocity gradient layer (>3 s^{-1}), corresponding to the base of layer 2A (Figures 2d and S7). Over the region, the typical thickness of layer 2A is ~600 m but it is measurably thicker, 700–900 m below the three summit edifices (Figures 2d, 2e, S2, and S7), and thinner ~300 m below the lava lake (Figures S2 and S7). In order to get a picture of the general differences between the three volcanic cones and the lava lake, we horizontally averaged velocity in these four areas (Figure 3a). The averaged velocity beneath the volcanic cones shows similar behavior down to 300 m below the seafloor, and is 15–20% lower than that beneath the lava lake (Figure 3b).

[8] Furthermore, time-to-depth conversion of the seismic reflection profiles using the 3D tomography velocities shows that the two main reflectors coincide well with the top and the bottom of the layer 2A gradient zone (Figures 2d and S7). However, the shallow reflector observed underneath the central volcano region can present some overlapping structures and seems to coincide well with the low

[1] Auxiliary materials are available in the HTML. doi:10.1029/2011GL047753.

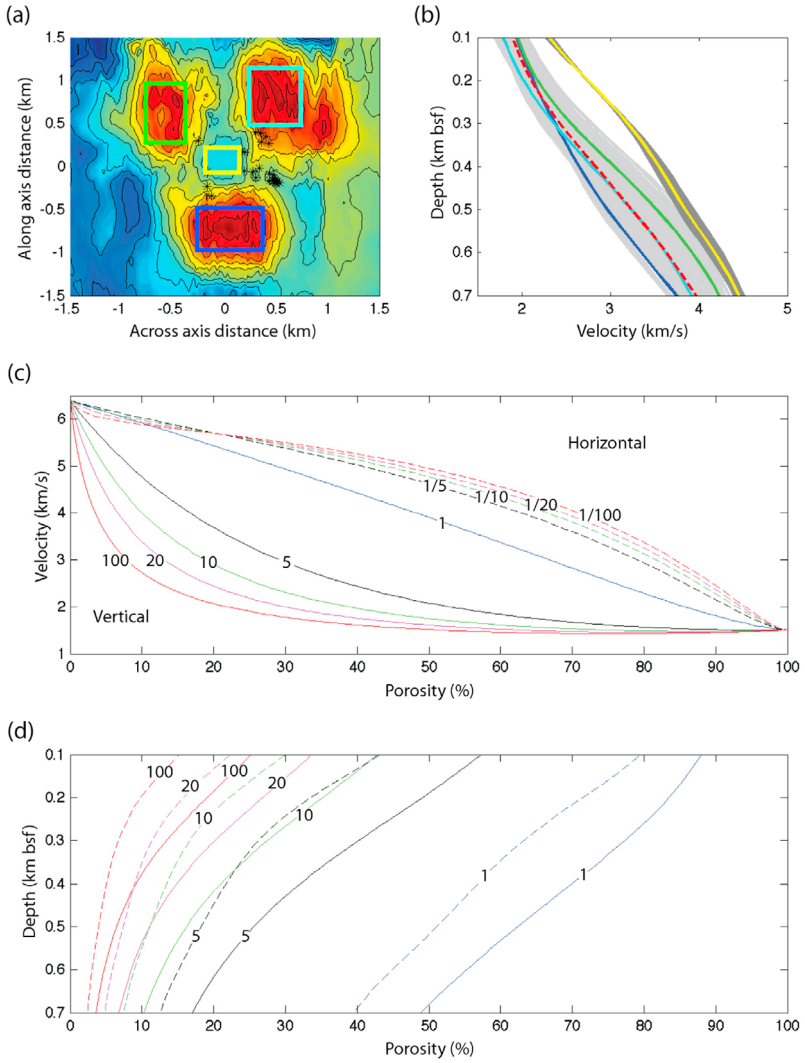

Figure 3. Porosity estimation. (a) Bathymetric map of the central part of the Lucky Strike volcano. Black stars mark the hydrothermal vents. Rectangles show the areas where velocity profiles have been studied. (b) Mean vertical velocity profiles (cyan, blue, green and yellow lines) for the areas shown in Figure 3a. The light gray and the dark gray areas correspond respectively to the velocity range underneath the volcanic cones and the lava lake. The red dashed line corresponds to the mean velocity through all the three summit cones. (c) Estimates of subsurface porosity using an aligned crack distribution and differential effective medium theory (DEMT). The number denotes the aspect ratio (the quotient of polar and equatorial radius). A value of 1 denotes spherical inclusions, and a value larger than 1 corresponds to prolate inclusions. For elliptical aligned inclusions, the velocity in the slow direction is represented by solid lines and the velocity in the fast direction is represented by dashed lines. (d) Subsurface porosity distribution estimated using aligned DEMT in the slow direction. The solid and dashed lines mark respectively the porosities at the volcanic cones and at the lava lake. The numbers give the inverse aspect ratio.

velocity zone (1.8 to 2.2 km.s^{-1}). It is therefore linked to the lower limit of different high porosity extrusive sequences (Figures 2c and 2e).

[9] We used a differential effective medium theory [*Berryman et al.*, 2002; *Taylor and Singh*, 2002] to estimate the porosity in layer 2A from its seismic velocity structure. We have assumed a two-phase effective medium consisting of basalt and seawater [*Seher et al.*, 2010b]. We compute the porosity as function of velocity for different aspect ratios. Spherical inclusions (aspect ratio 1) would require an unrealistically high porosity (>80%) (Figure 3c). Vertically aligned ellipsoids with aspect ratios between 5 and 100 can better explain the observed low velocities. At 100 m below the seafloor (bsf), porosity beneath the volcanic cones would be between 25% and 57%, but only between 15% and 43% below the lava lake (Figure 3d). At 700 m bsf, the respective porosities are reduced to 4–17% and 3–12%. The difference in the velocities beneath lava lake and the volcanic cones can be explained by a change in the crack aspect ratio between these different domains or modification in the porosity. Thus a decrease in the fault concentration between the volcanic cones and the lava lake of 11–14% at 100 m bsf and 2–5% at 700 m bsf would be sufficient to explain the change in the seismic velocities, and this difference in

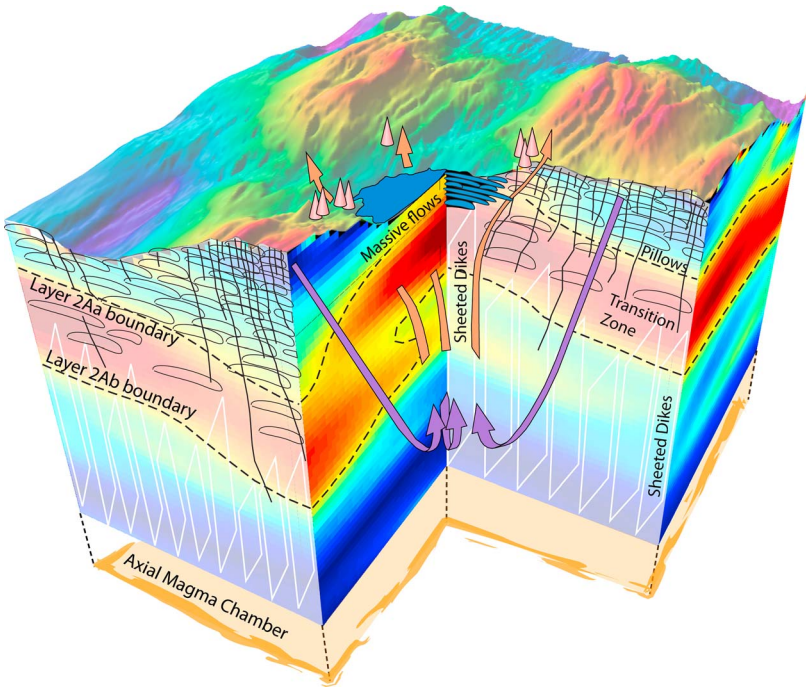

Figure 4. Three-dimensional schematic view of the shallow crust. Schematic diagram relating different features observed in seismic image to the bathymetry. The background represents a 3D view of the vertical velocity gradient. Beneath the three volcanic cones porous and highly fractured pillow lava layers are inferred down to 600 m. In addition, 500 m away from these three volcanic edifices, the shallow crust beneath the lava lake is formed by thinner and less porous lava flows. The hydrothermal vents (pink cones) seem to lie at the permeability interface between lava flows and pillows.

fault concentration is consistent with seafloor observations [*Humphris et al.*, 2002]. Furthermore, porosities between 25–35%, related to cracks with aspect ratio of 20–100, are consistent with other independent measures of porosity (25–30%) that have been made with on-bottom gravimeters [*Gilbert and Johnson*, 1999; *Gilbert et al.*, 2007; *Cochran et al.*, 1999]. Finally, differences in nature of lavas between a possible intrusive dike underneath massive flows at lava lake location and pillow lavas with high inherent porosity at volcanic edifices could also explained the differences in porosity observed at these two locations.

4. Conclusions

[10] We observe a thick layer 2A and higher density of faults beneath the three volcanic cones [*Humphris et al.*, 2002] and a thin layer 2A beneath the geologically different lava lake, combined with the presence of the hydrothermal vents lying between these two structures. These results have important implications for our understanding of magmatic-tectonic-hydrothermal interactions at slow-spreading ridges. Figure 4 presents a schematic diagram summarizing the three-dimensional geometry of the young shallow crust. Upper crustal porosity appears to be affected by both magmatic accretion (that can be expressed in different ways at pillow lava mounds or flat lava lake) and extensive tectonism (faults, cracks and fissures). Interestingly, the hydrothermal vents seem to lie around the lava lake, at the boundary between the relatively low porosity lava lake and the high porosity volcanic cones, and above the observed axial magma chamber reflection [*Singh et al.*, 2006a]. It seems that contrasts in fracture density, in lava emplacement, and thus in porosity and permeability determine the location of the up flow arms of the hydrothermal circulation, while the high porosity volcanic cones may act as sinks (Figure 4). A compact local hydrothermal circulation model is in good agreement with a sheet flow cap model [*Humphris et al.*, 2002] and with recent numerical simulations [*Coumou et al.*, 2008]. Indeed, a pipe like up-flow zone surrounded by narrow zones of focused down-flow promotes heat exchange between the two arms of the circulation maximizing the energy transport. Our results have demonstrated the necessity of using a high-resolution, three dimensional technique such as downward continuation, combined with three dimensional tomography to image highly variable and complex oceanic crust, which could help to resolve the inconsistency between the surface geological observations and geophysical imaging [*Christeson et al.*, 2007].

[11] **Acknowledgments.** We are grateful to the captain, crew and seismic team from GENAVIR of cruise SISMOMAR of the RV *l'Atalante* for their assistance. We also thank Tim Seher for his insights along this work. This study also benefited from reviews by Harm Van Avendonk and an anonymous reviewer. The INSU MOMAR program funded the acquisition of SISMOMAR project. This is an Institut de Physique du Globe de Paris contribution. This work was also supported by the National Science Foundation by grant OCE-0826481.

[12] The Editor thanks Harm J. A.Van Avendonk and Ingo Grevemeyer for their assistance in evaluating this paper.

References

Berryhill, J. R. (1984), Wave-equation datuming before stack, *Geophysics*, *49*, 2064–2066, doi:10.1190/1.1441620.

Berryman, J., S. Pride, and H. Wang (2002), A differential scheme for elastic properties of rocks with dry or saturated cracks, *Geophys. J. Int.*, *151*, 597–611, doi:10.1046/j.1365-246X.2002.01801.x.

Christeson, G., G. Purdy, and G. Fryer (1994), Seismic constraints on shallow crustal emplacement processes at the fast spreading East Pacific Rise, *J. Geophys. Res.*, *99*, 17,957–17,973, doi:10.1029/94JB01252.

Christeson, G. L., K. D. McIntosh, and J. A. Karson (2007), Inconsistent correlation of seismic layer 2a and lava layer thickness in oceanic crust, *Nature*, *445*, 418–421, doi:10.1038/nature05517.

Cochran, R., D. J. Fornari, B. J. Coakley, R. Herr, and M. A. Tivey (1999), Continuous near-bottom gravity measurements made with a BGM-3 gravimeter in DSV Alvin on the East Pacific Rise crest near 9°31′N and 9°50′N, *J. Geophys. Res.*, *104*, 10,841–10,861, doi:10.1029/1999JB900049.

Collins, J. A., D. K. Blackman, A. Harris, and R. L. Carlson (2009), Seismic and drilling constraints on velocity structure and reflectivity near IODP Hole U1309D on the central dome of Atlantis Massif, Mid-Atlantic Ridge 30°N, *Geochem. Geophys. Geosyst.*, *10*, Q01010, doi:10.1029/2008GC002121.

Combier, V. (2007), Mid-ocean ridge processes. Insights from 3D reflection seismics at 9°N OSC on the East Pacific Rise, and the Lucky Strike Volcano on the Mid-Atlantic Ridges, Ph.D. thesis, Lab. de Geosci. Mar., Inst. de Phys. du Globe de Paris, Paris.

Coumou, D., T. Driesner, and C. A. Heinrich (2008), The structure and dynamics of Mid-Ocean Ridge hydrothermal systems, *Science*, *321*, 1825–1828, doi:10.1126/science.1159582.

DeMets, C., R. G. Gordon, D. F. Argus, and S. Stein (1994), Effect of recent revisions to the geomagnetic reversal timescale on estimates of current plate motions, *Geophys. Res. Lett.*, *21*, 2191–2194, doi:10.1029/94GL02118.

Detrick, R. S., H. D. Needham, and V. Renard (1995), Gravity anomalies and crustal thickness variations along the Mid-Atlantic Ridge between 33°N and 40°N, *J. Geophys. Res.*, *100*, 3767–3787, doi:10.1029/94JB02649.

Gilbert, L. A., and H. P. Johnson (1999), Direct measurements of oceanic crustal density at the northern Juan de Fuca Ridge, *Geophys. Res. Lett.*, *26*, 3633–3636, doi:10.1029/1999GL008391.

Gilbert, L. A., R. E. McDuff, and H. P. Johnson (2007), Porosity of the upper edifice Axial Seamount, *Geology*, *35*, 49–52, doi:10.1130/G22892A.1.

Harding, A. J., G. M. Kent, and J. A. Orcutt (1993), A multichannel seismic investigation of the upper crustal structure at 9°N on the East Pacific Rise: Implications for crustal accretion, *J. Geophys. Res.*, *98*, 13,925–13,944, doi:10.1029/93JB00886.

Harding, A. J., G. M. Kent, D. K. Blackman, S. C. Singh and J-P. Cannales (2007), A new method for MCS refraction data analysis of the uppermost section at a Mid-Atlantic Ridge core complex, *Eos Trans. AGU*, *88*(52), Fall Meet. Suppl., Abstract S12A–03.

Humphris, S. E., D. J. Fornari, D. S. Scheirer, C. R. German, and L. M. Parson (2002), Geotectonic setting of hydrothermal activity on the summit of Lucky Strike Seamount (37°17′N, Mid-Atlantic Ridge), *Geochem. Geophys. Geosyst.*, *3*(8), 1049, doi:10.1029/2001GC000284.

Kent, G. M., et al. (2000), Evidence from three-dimensional seismic reflectivity images for enhanced melt supply beneath mid-ocean-ridge discontinuities, *Nature*, *406*, 614–618, doi:10.1038/35020543.

Langmuir, C., et al. (1997), Hydrothermal vents near a mantle hot spot: The Lucky Strike vent field at 37°N on the Mid-Atlantic Ridge, *Earth Planet. Sci. Lett.*, *148*, 69–91, doi:10.1016/S0012-821X(97)00027-7.

Ondréas, H., Y. Fouquet, M. Voisset, and J. Radford-Knoery (1997), Detailed study of three contiguous segments of the Mid-Atlantic Ridge, south of the Azores (37°N to 38°30′N), using acoustic imaging coupled with submersible observations, *Mar. Geophys. Res.*, *19*, 231–255, doi:10.1023/A:1004230708943.

Ondréas, H., M. Cannat, Y. Fouquet, A. Normand, P. M. Sarradin, and J. Sarrazin (2009), Recent volcanic events and the distribution of hydrothermal venting at the Lucky Strike hydrothermal field, Mid-Atlantic Ridge, *Geochem. Geophys. Geosyst.*, *10*, Q02006, doi:10.1029/2008GC002171.

Seher, T., W. C. Crawford, S. C. Singh, M. Cannat, V. Combier, and D. Dusunur (2010a), Crustal velocity structure of the Lucky Strike segment of the Mid-Atlantic Ridge at 37°N from seismic refraction measurements, *J. Geophys. Res.*, *115*, B03103, doi:10.1029/2009JB006650.

Seher, T., S. C. Singh, W. Crawford, and J. Escartin (2010b), Upper crustal velocity structure beneath the central Lucky Strike Segment from seismic refraction measurements, *Geochem. Geophys. Geosyst.*, *11*, Q05001, doi:10.1029/2009GC002894.

Singh, S. C., et al. (2006a), Discovery of a magma chamber and faults beneath a Mid-Atlantic Ridge hydrothermal field, *Nature*, *442*, 1029–1032, doi:10.1038/nature05105.

Singh, S. C., et al. (2006b), Seismic reflection images of the Moho underlying melt sills at the East Pacific Rise, *Nature*, *442*, 287–290, doi:10.1038/nature04939.

Taylor, M., and S. C. Singh (2002), Composition and microstructure of magma bodies from effective medium theory, *Geophys. J. Int.*, *149*, 15–21, doi:10.1046/j.1365-246X.2002.01577.x.

A. F. Arnulf, W. Crawford, and S. C. Singh, Laboratoire de Géosciences Marines, Institut de Physique du Globe de Paris, 1 rue Jussieu, F-75238 Paris CEDEX 05, France. (arnulf@ipgp.fr)

A. J. Harding, Cecil H. and Ida M. Green Institute of Geophysics and Planetary Physics, University of California, San Diego, La Jolla, CA 92093, USA.

G. M. Kent, Nevada Seismological Laboratory, University of Nevada, Reno/0174, Reno, NV 89557, USA.